Ocean Heat Content Estimates from Ocean Reanalyses since 1993

Haohao Zhang[1], Andrea Storto[2], Lijing Cheng[1], Romain Bourdallé-Badie[3], Satoshi Osafune[4], Andrea Cipollone[5], Caihong Wen[6], James A. Carton[7], Gaël Forget[8], Yuying Pan[1], Marie Drevillon[3], Karina von Schuckmann[3], Magdalena A. Balsamda[9], Matthew A. Chamberlain[10], Chunxue Yang[*2]

[1]State Key Laboratory of Earth System Numerical Modeling and Application, Institute of Atmospheric Physics, Chinese Academy of Sciences, Beijing 100029, China

[2]Institute of Marine Sciences (ISMAR), National Research Council of Italy (CNR), Via del Fosso del Cavaliere 100, 00133 Rome, Italy

[3]Mercator Ocean International, Toulouse, France

[4]Research Institute for Global Change (RIGC), Japan Agency for Marine-Earth Science and Technology (JAMSTEC), Yokosuka 237-0061, Japan

[5]CMCC Foundation—Euro-Mediterranean Center on Climate Change, Bologna, Italy

[6]Climate Prediction Center, National Centers for Environmental Prediction, National Weather Service, NOAA, College Park, MD 20740, USA

[7]Department of Atmospheric and Oceanic Science, University of Maryland, College Park, MD 20742, USA

[8]Department of Earth, Atmospheric and Planetary Sciences, Massachusetts Institute of Technology, Cambridge, MA 02139, USA

[9]Research Department, European Centre for Medium-Range Weather Forecasts (ECMWF), Reading, United Kingdom

[10]CSIRO Environment, Hobart, TAS, Australia

Correspondence to: Chunxue Yang (chunxue.yang@cnr.it)

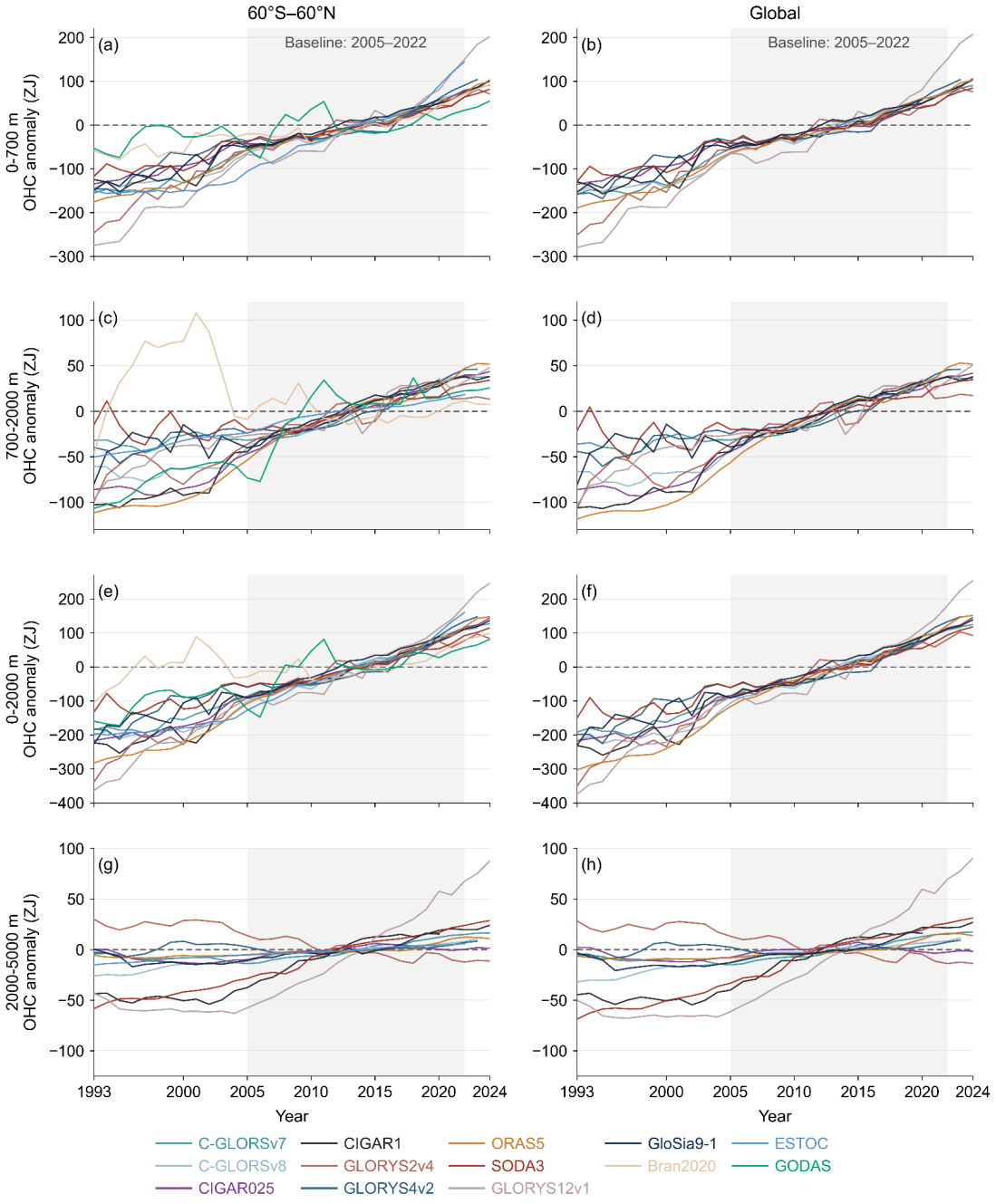


Figure S1. Individual ORA OHC anomalies. Annual OHC anomalies are shown for 13 ORA products in 0–700 m, 700–2000 m, 0–2000 m and 2000–5000 m. Left panels show 60°S–60°N, and right panels show global OHC. Anomalies are referenced to 2005–2022, except for GloSia9-1, for which 2005–2020 is used because its data end in 2020.

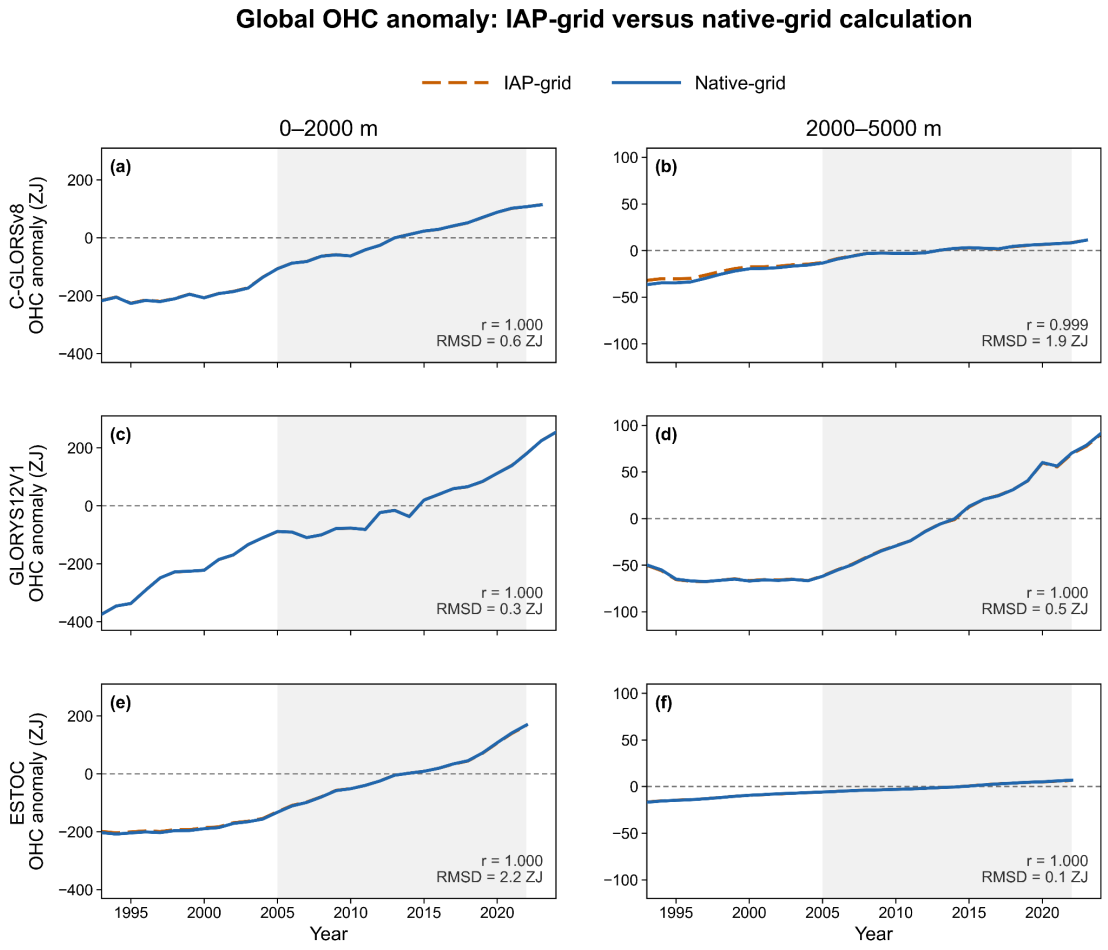


Figure S2. Sensitivity of global OHC anomalies to interpolation onto the common IAP grid. Rows show C-GLORSv8, GLORYS12v1, and ESTOC. Left and right columns show 0–2000 m and 2000–5000 m, respectively. Blue solid lines show OHC calculated on each product's native grid, and orange dashed lines show OHC calculated after interpolation onto the IAP grid. Anomalies are referenced to 2005–2022. Values indicate the Pearson correlation coefficient (r) and root-mean-square difference (RMSD) between the two time series.

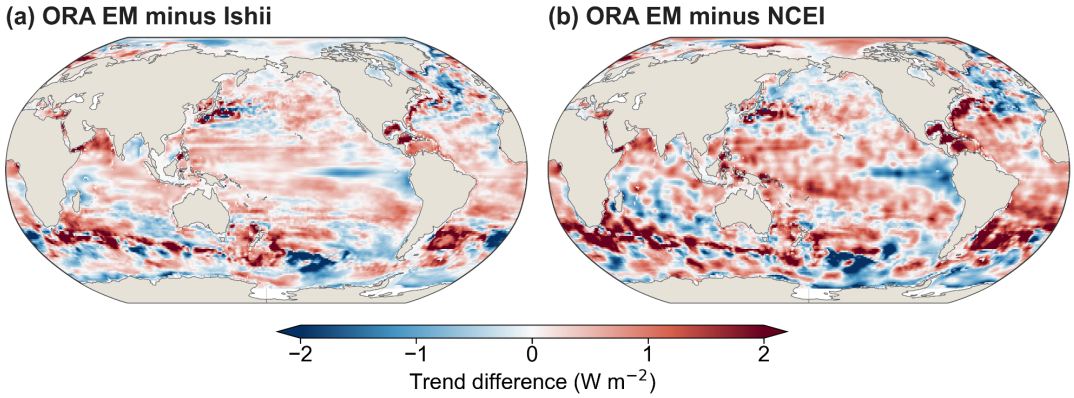


Figure S3. Differences between the ORA EM and OA 0–2000 m OHC trends during 1993–2022. Panels (a,b) show ORA EM minus Ishii and NCEI, respectively.

45

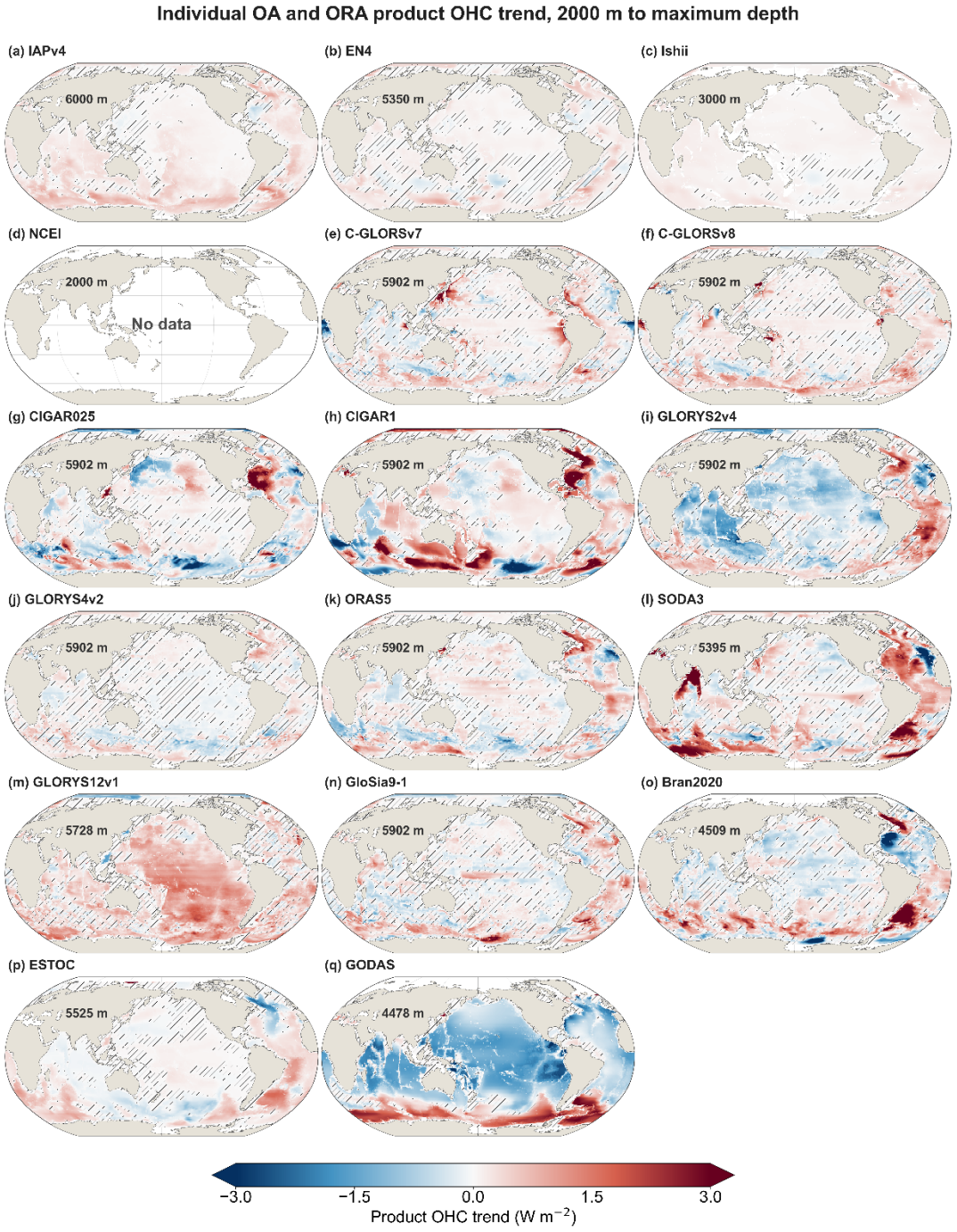
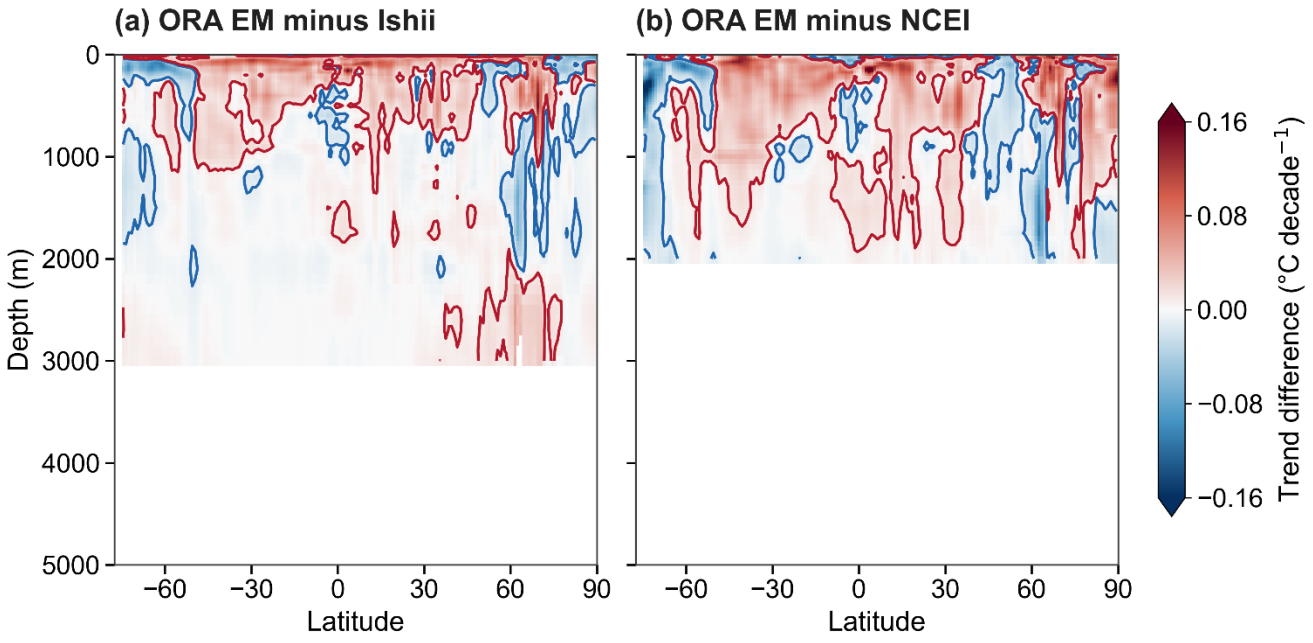


Figure S4. Individual OA and ORA deep-ocean OHC trends. Panels (a–d) show the four OA products, and panels (e–q) show the individual ORA products. Trends are calculated from 2000 m to each product's maximum available depth over 1993–2022, except for GloSia9-1, for which 1993–2020 is used because its data end in 2020. Hatching marks grid cells where the linear trend is not statistically significant at the 90% confidence level. Ishii and NCEI are blank because they do not provide data below 2000 m.



55 **Figure S5. Latitude–depth differences in zonal-mean temperature trends during 1993–2022. Panels (a,b) show ORA EM minus Ishii and NCEI, respectively. Blue and red contours mark −0.01 and +0.01 °C decade^{-1}, respectively.**

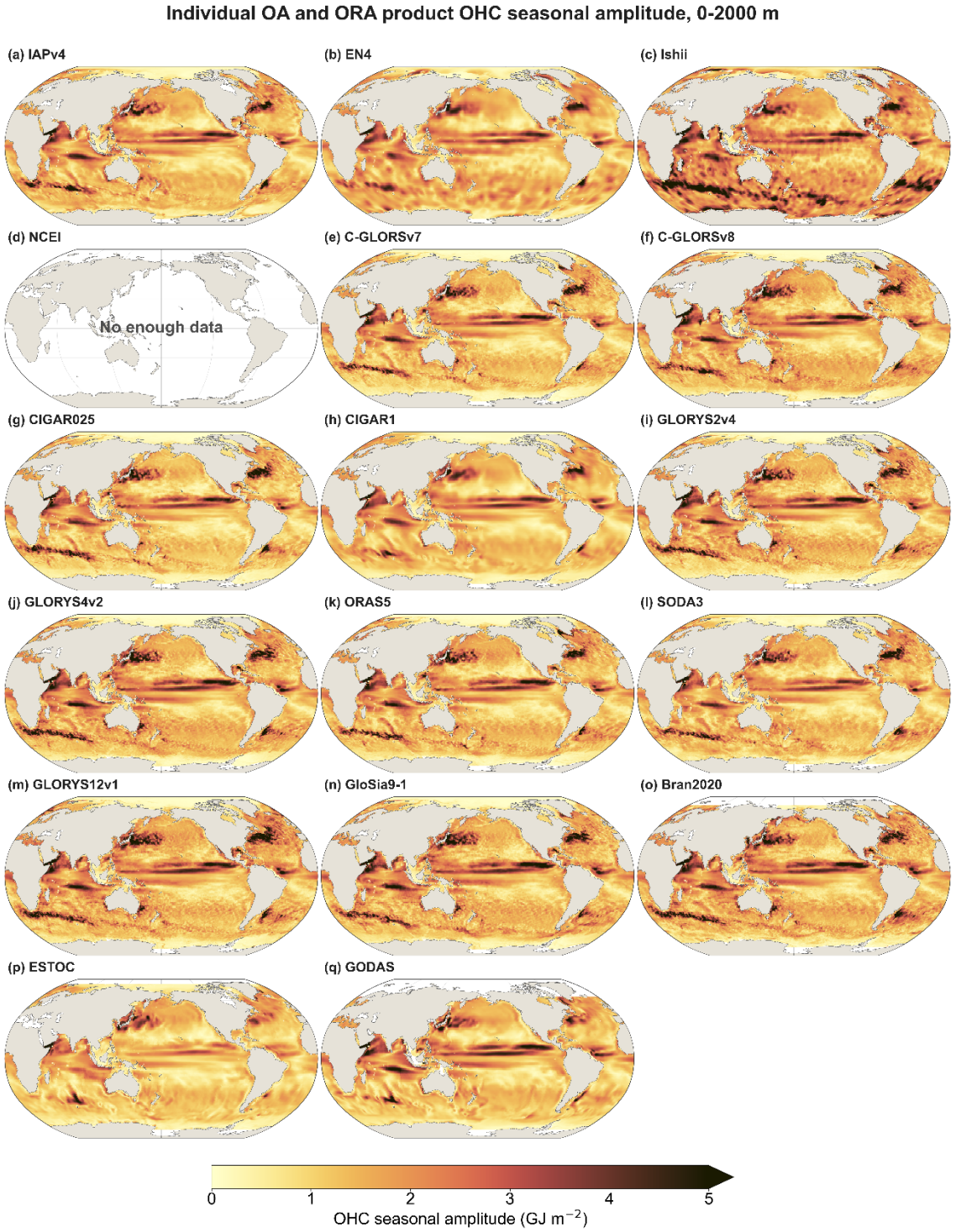


Figure S6. Seasonal-cycle amplitude of 0–2000 m OHC in individual OA and ORA products. Panels (a–d) show the four OA products, and panels (e–q) show the individual ORA products.

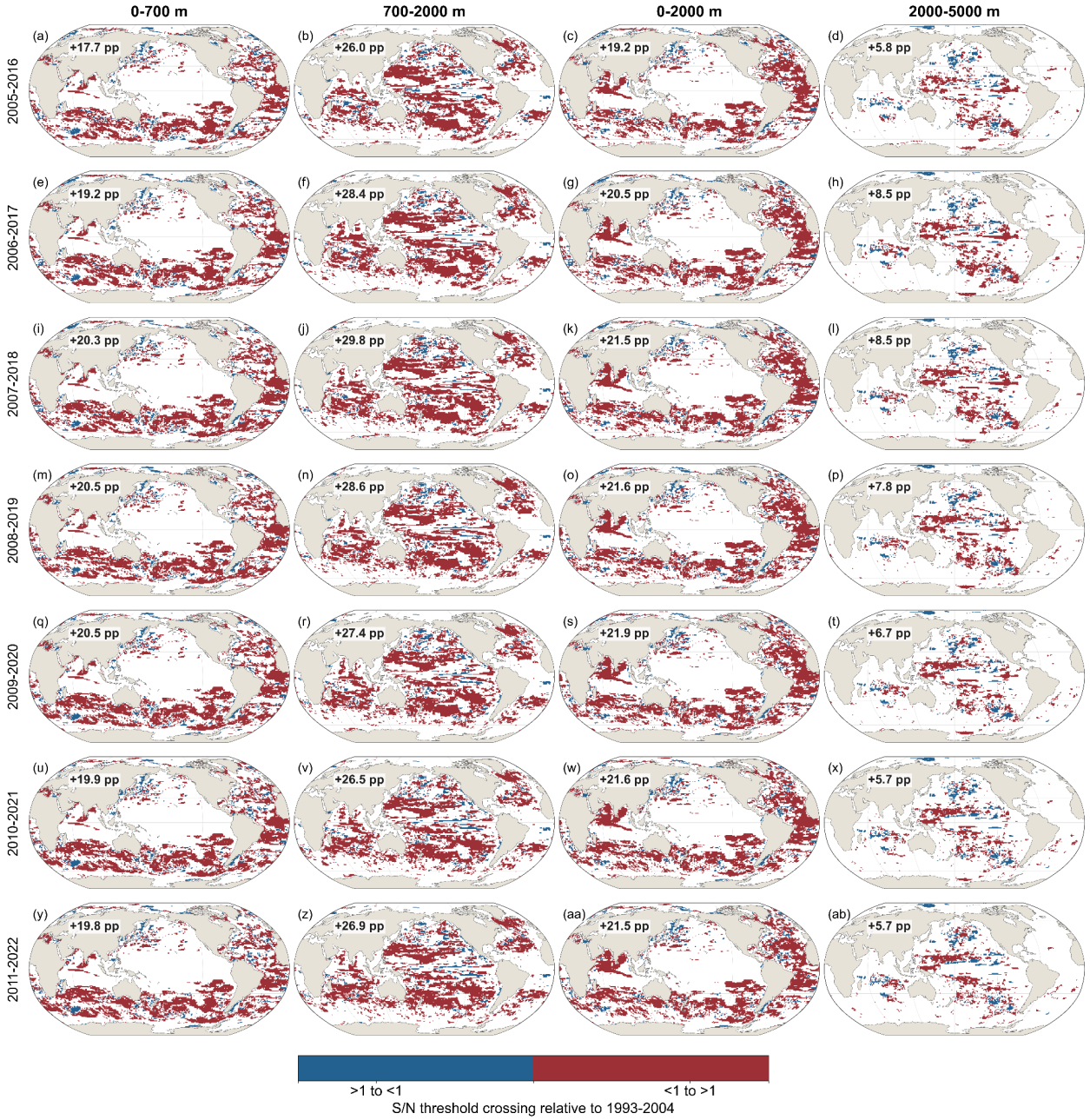


Figure S7. Sensitivity of ORA OHC interannual S/N changes to the choice of 12-year post-Argo period. Rows show seven 12-year periods from 2005–2016 to 2011–2022, and columns show 0–700 m, 700–2000 m, 0–2000 m, and 2000–5000 m, respectively. Each period is compared with 1993–2004. Red marks changes from S/N < 1 in 1993–2004 to S/N > 1 in the corresponding post-Argo period, and blue marks the reverse. Percentage labels indicate changes in the ocean-area fraction with S/N > 1 in percentage points (pp).

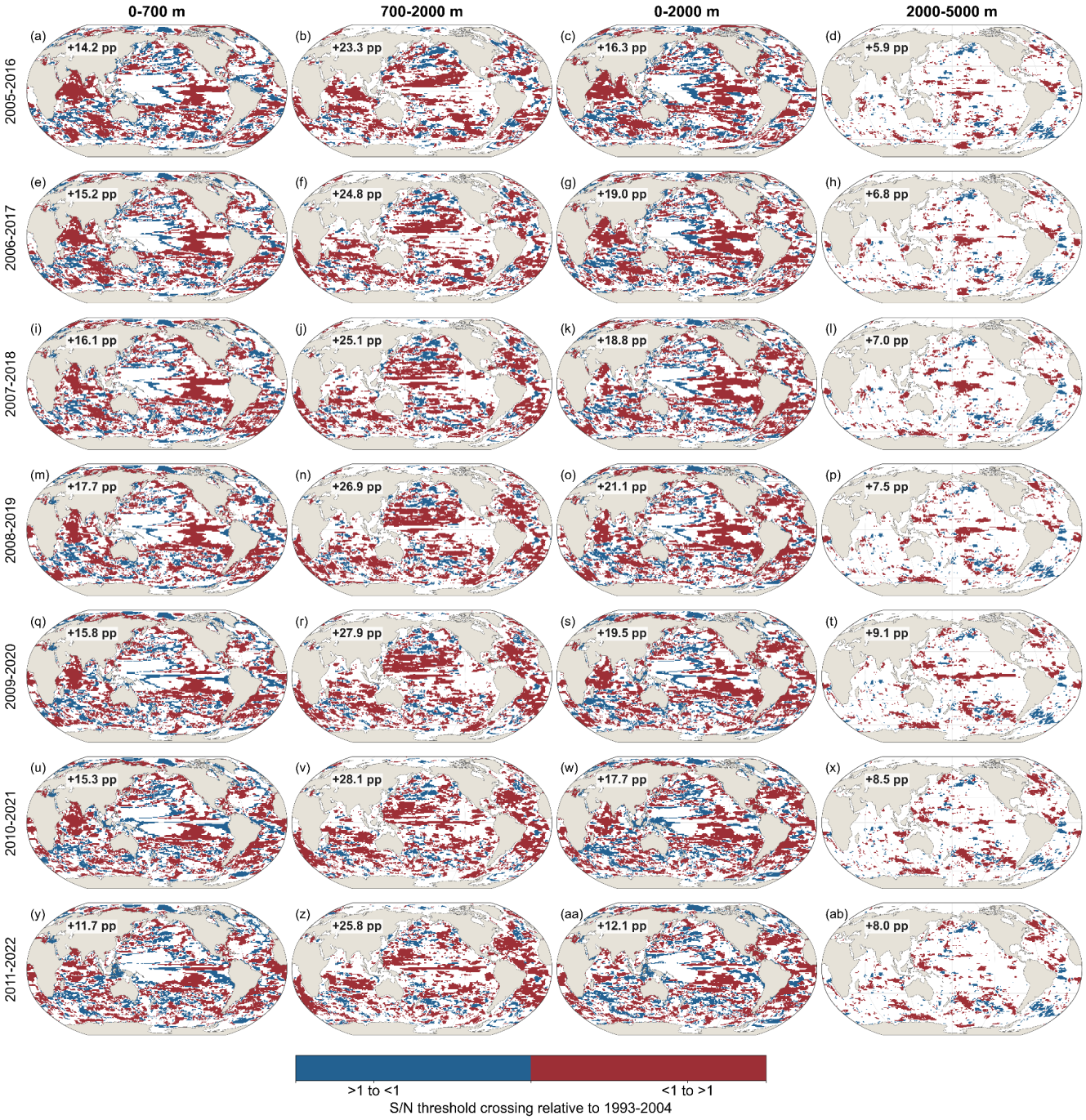


Figure S8. Same as Figure S7, but for ORA OHC trend S/N.

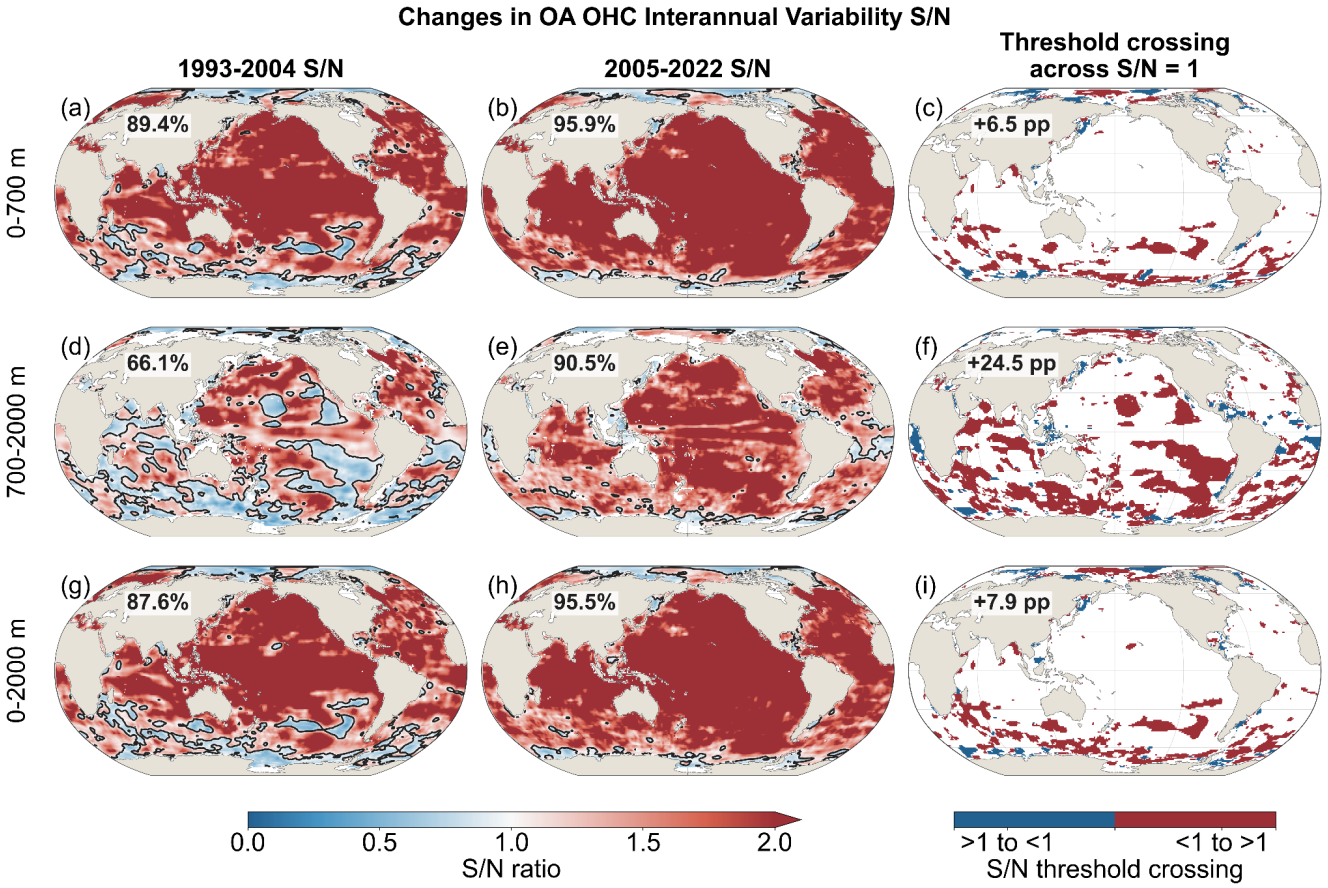


Figure S9. Changes in OA OHC interannual S/N across the Argo transition. Rows show 0–700 m, 700–2000 m, and 0–2000 m, respectively. The first two columns show S/N for 1993–2004 and 2005–2022, respectively, and the third column shows crossings of the S/N = 1 threshold. Black contours mark S/N = 1. Percentage labels in the first two columns indicate the valid ocean area with S/N > 1. In the third column, numbers indicate changes in the ocean-area fraction with S/N > 1 in percentage points (pp).

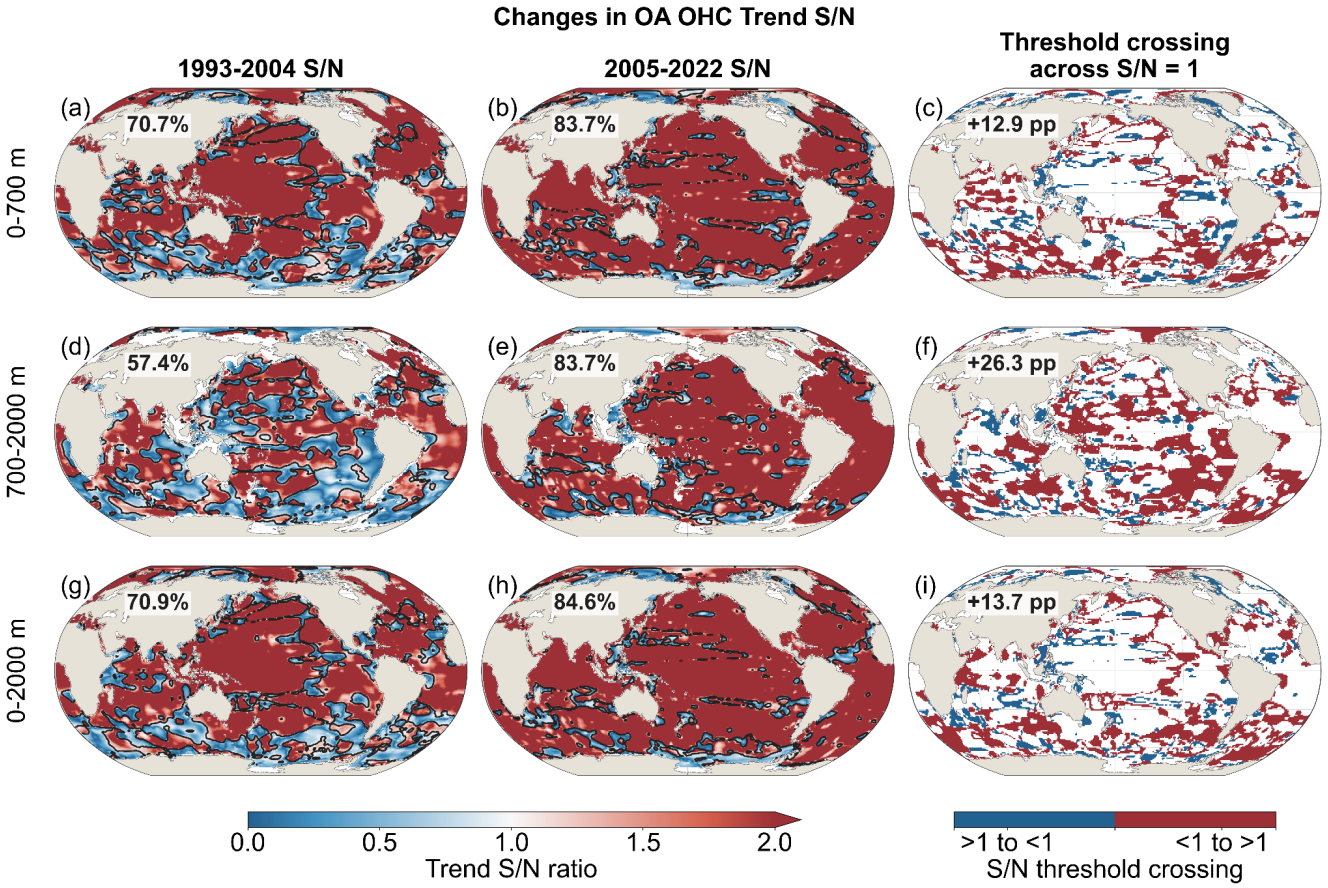


Figure S10. Same as Figure S9, but for OA OHC trend S/N.

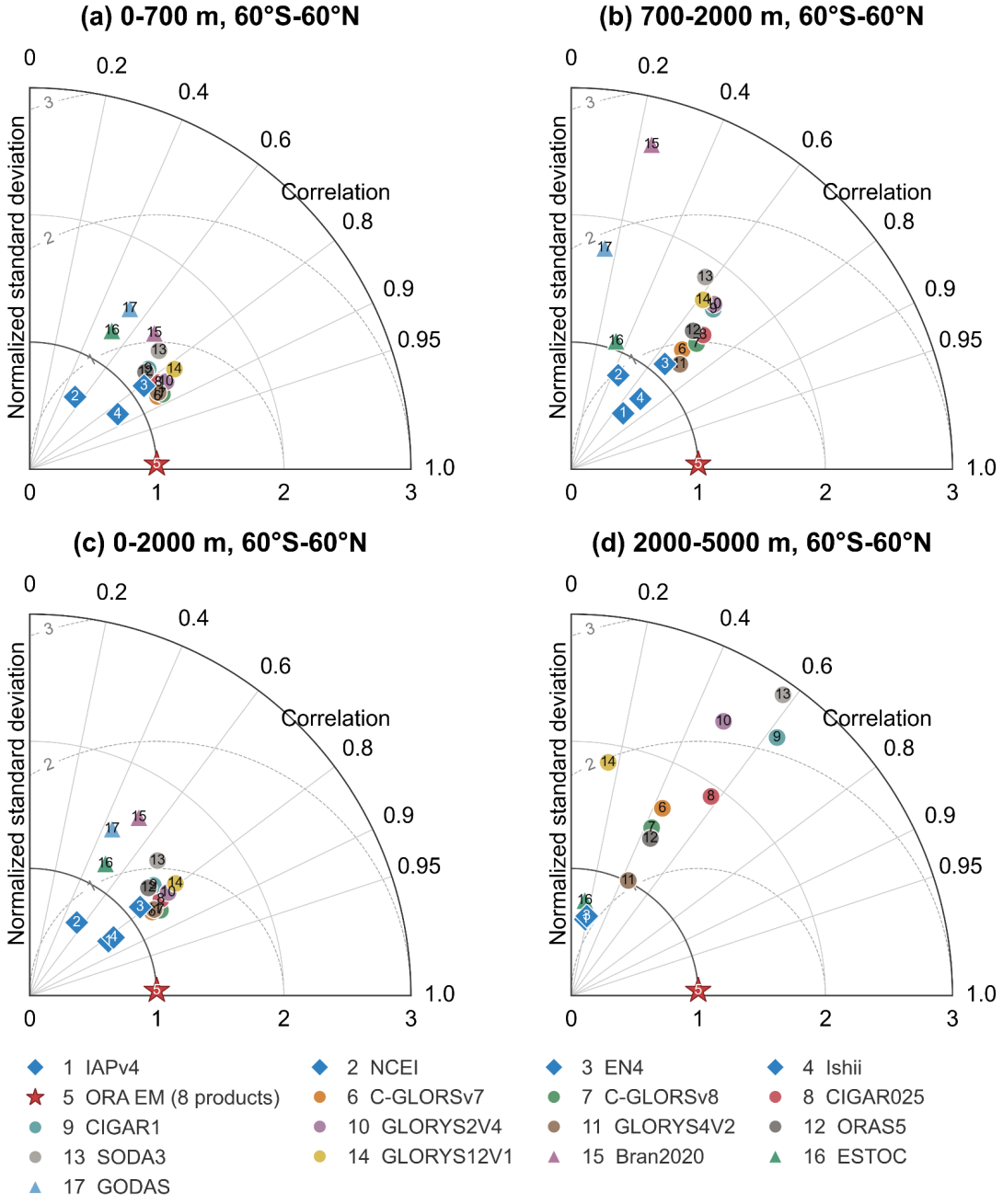


Figure S11. Taylor-diagram comparison of OHC anomalies against the ORA EM over 60°S–60°N. Panels (a–d) show 0–700 m, 700–2000 m, 0–2000 m, and 2000–5000 m, respectively. Metrics are calculated from annual OHC anomalies relative to each product's 2005–2022 mean. Angular position indicates the correlation with the ORA EM, radial distance indicates the standard deviation normalized by that of the ORA EM, and grey dashed arcs indicate the normalized centered root-mean-square difference. The red star marks the ORA EM, blue diamonds denote OA products, and circles and triangles denote individual ORA products.